This is an *Accepted Manuscript*, which has been through the Royal Society of Chemistry peer review process and has been accepted for publication.

Accepted Manuscripts are published online shortly after acceptance, before technical editing, formatting and proof reading. Using this free service, authors can make their results available to the community, in citable form, before we publish the edited article. We will replace this *Accepted Manuscript* with the edited and formatted *Advance Article* as soon as it is available.

You can find more information about *Accepted Manuscripts* in the **Information for Authors**.

Journal Name

ARTICLE

Polyethylenimine promoted electrocatalytic reduction of CO_2 to CO in aqueous medium by graphene-supported amorphous molybdenum sulphide

Fengwang Li,[a,b] Shu-Feng Zhao,[a,c] Lu Chen,[a] Azam Khan,[a,d] Douglas R. MacFarlane[a,b*] and Jie Zhang[a,b*]

Abstract: Efficiently and selectively converting CO_2 to value-added carbon compounds remains a major challenge in sustainable energy research. In this paper, we report the synthsis of a cost-effective catalyst, i.e. amorphous molybdenum sulphide on a polyethylenimine modified reduced graphene oxide substrate, for electrocatalytically reducing CO_2 into CO in CO_2 saturated aqueous $NaHCO_3$ medium with high efficiency and selectivity. The catalyst is capable of producing CO at overpotentials as low as 140 mV and reaches a maximum faradaic efficiency of 85.1% at an overpotential of 540 mV. At an overpotential of 290 mV with respect to the formation of CO, it catalyzes the formation of syngas with high stability. Detailed investigations reveal that PEI works as a co-catalyst by providing a synergetic effect with MoS_x.

Broader context: Electrochemical CO_2 reduction using renewable energy as a power source could potentially solve the energy and environmental problems arising from excessive use of non-renewable fossil fuels. Currently, electrocatalysts for this reaction generally suffer from high cost, low energetic efficiency and poor product selectivity. Nevertheless, molybdenum or tungsten containing formate dehydrogenases (FDH) can efficiently and selectively catalyze reduction of CO_2 to formate in Nature. Inspired by the active sites of FDH, amorphous molybdenum sulphide (MoS_x) on a polyethylenimine (PEI) modified reduced graphene oxide (rGO) substrate has been synthesized and used as a heterogeneous electrocatalyst for reduction of CO_2 to CO in aqueous medium. The high efficiency and selectivity is accomplished by the synergetic effect of MoS_x and PEI while rGO improves electrical conductivity and stability of the catalyst.

Introduction

Energy and environmental problems are among the most challenging issues facing mankind in this century.[1-3] Despite tremendous efforts to develop renewable energy sources, the majority of energy used today is still from non-renewable, fossil fuel sources, which leads to an increase in greenhouse CO_2 levels in the atmosphere and may cause catastrophic climate changes. Electrocatalytic reduction of CO_2, which recycles CO_2 back to fuels and commodity chemicals by using renewable energy as a power source, could provide an attractive solution to this issue.[4] However, CO_2 is very stable under environmental conditions and the hydrogen evolution reaction (HER) often prevails over CO_2 reduction in aqueous electrolytes under cathodic polarization,[5,6] making it essential to find a suitable catalyst to achieve cost-effective CO_2 reduction with high efficiency and selectivity.

The past several decades have witnessed reports of a number of homogeneous and heterogeneous catalysts for electrocatalytic CO_2 reduction; these mainly include metals,[5] metal oxides,[7-9] metal complexes[10-13] and nitrogen-containing carbon materials[14-17]. Among them, noble metals such as Au, Ag and Pd have attracted particular interest for they can selectively convert CO_2 to CO at relatively low overpotentials.[5,18] Moreover, nanostructured noble metals have been developed recently to enhance their performance.[19-27] For example, oxide-derived Au nanoparticles exhibit highly selective CO_2 reduction to CO in aqueous solution at a lower overpotential than a polycrystalline bulk Au electrode.[20] However, precious metals are hampered by their low abundance and high cost, which restrict their practical, large-scale application. Thus, searching for abundant and efficient electrocatalysts with selectivity towards CO, or capable of producing syngas that could be readily utilized in a Fischer-Tropsch process, is vital for commercializing CO_2 electroreduction technologies.[28] Although less expensive materials such as Cu, Sn, Bi and their oxides have

a. School of Chemistry, Monash University, Clayton 3800, Victoria, Australia. Email: jie.zhang@monash.edu; douglas.macfarlane@monash.edu
b. ARC Centre of Excellence for Electromaterials Science, School of Chemistry, Monash University, Clayton 3800, Victoria, Australia.
c. CSIRO Process Science and Engineering, Box 312, Clayton South 3168, Victoria, Australia
d. Department of Chemistry, Quaid-i-Azam University, Islamabad 45320, Pakistan.
Electronic Supplementary Information (ESI) available. See DOI: 10.1039/x0xx00000x

demonstrated promise for reduction of CO_2 to hydrocarbons, formic acid and CO,[29-32] these systems generally show low activities and/or selectivity for CO production or need non-aqueous solvents which may limit their practical applications.

In Nature, formate dehydrogenases (FDH), which contain molybdenum or tungsten centers coordinated by a selenocysteine residue and amino acid residues, can catalyze the oxidation of formate to CO2.[33,34] Hirst and co-workers[35,36] showed that they could efficiently and specifically catalyze the reversible transformation between CO_2 and formate under mild conditions. This inspires us to explore new catalysts resembling the FDH active site for electroreduction of CO_2. Molybdenum disulphide (MoS_2), a two-dimensional transition metal dichalcogenide, has sparked tremendous research interest as a substitute for Pt for effectively catalysing the HER in acidic media.[37-40] MoS_2 consists of a planar triangular lattice of Mo atoms sandwiched between two planes of S atoms and each Mo (IV) is coordinated to six S ligands, while each S center is connected to three Mo atoms. From a biomimic point of view, MoS_2 shares a similar structure with the active center of FDH, making it potentially an electrocatalyst for CO_2 reduction. Recently, Nørskov *et al.*[41] demonstrated theoretically that MoS_2 could possibly be an electrocatalyst for CO_2 reduction and this was subsequently proven experimentally in ionic liquid (IL) medium with water as a proton source.[42] In the present work we demonstrate that amorphous molybdenum sulphide (MoS_x) on a polyethylenimine (PEI) modified reduced graphene oxide (rGO) substrate can be a highly efficient and selective electrocatalyst for reduction of CO_2 to CO in simple aqueous medium at low overpotentials. We show that the PEI layer considerably enhances the catalytic activity of the MoS_x, presumably by suppressing HER and stabilising the $CO_2^{.-}$ intermediate during CO_2 reduction, as has been suggested previously for PEI on carbon nanotube materials.[43]

Experimental

Chemicals and apparatus

$NaHCO_3$ (ACS grade), NaOH and NaH_2PO_4 (AR grade) were purchased from Merck. Natural graphite (crystalline, 300 mesh) was from Alfa Aesar. Polyethylenimine (PEI, M_n = 10,000, branched), polyethylene glycol (PEG, M_n = 400), polydiallyldimethylammonium chloride (PDDA, 20 wt% in water, M_w = 100,000 ~ 200,000) and $(NH_4)_2MoS_4$ (99.97% trace metals basis) were purchased from Sigma-Aldrich. All the chemicals were used without further purification. Graphene oxide (GO) was synthesized from natural graphite using the method described by Hummers *et al.*[44] Phosphate buffer was prepared by adding 5.0 M NaOH solution to 0.1 M NaH_2PO_4 solution to adjust the pH to 6.81. All the aqueous solutions were prepared with MilliQ water.
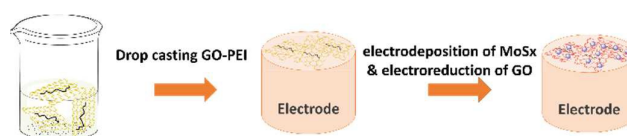
Fig. 1 Schematic illustration of the fabrication of rGO-PEI-MoS_x modified electrodes.

Transmission electron microscopic (TEM) images were collected on a FEI Tecnai G2 T20 TWIN TEM Instrument. Scanning electron microscopic (SEM) images and energy dispersive spectrum (EDS) were recorded on a FEI Nova NanoSEM 450 FEG SEM Instrument equipped with Bruker Quantax 400 X-ray analysis system. Raman spectra were obtained using a Renishaw inVia Microscope with a 532 nm laser source and IR spectra with a Digilab (7000) Stingray Imaging FT-IR Spectrometer. X-ray Diffraction (XRD) data were collected with a Philip X-ray powder diffractometer (Cu K_α radiation). Gas chromatography (GC) was performed with an Agilent 7820 A gas chromatography system equipped with a HP-plot molesieve (5A) column and a thermal conductivity detector (TCD). The carrier gas was helium (99.99%) for CO analysis while nitrogen (99.99%) was used as carrier gas for H_2 analysis. The retention times were compared with known compounds. All the electrochemical experiments were conducted on a CHI 760E electrochemical workstation (CH Instruments, Austin, Texas, USA) at room temperature (22 ± 2 °C).

Fabrication of rGO-PEI-MoS_x electrode

10 mg graphene oxide (GO) powder was dispersed in 10 mL water and pH was adjusted to around 9.0 by adding an appropriate amount of aqueous NaOH solution (5.0 M) dropwise. After sonication for at least 1 hour, 500 μL of a 5 wt% PEI aqueous solution was then added into the GO dispersion quickly and sonicated for another 30 minutes. Afterwards, it was stirred at 60 °C for 12 hours to form the GO-PEI solution. In order to obtain a well-dispersed solution, centrifugation at 3000 rpm was applied for 20 minutes to remove any large aggregates. The procedure for fabricating the rGO-PEI-MoS_x electrode is schematically described in Fig. 1. Firstly, 4 μl of GO-PEI solution was casted onto a glassy carbon electrode (GCE, 3 mm in diameter, CH Instruments, USA) to form the GO-PEI modified GCE and dried under an infrared lamp. The as-prepared electrode was then immersed into a solution composed of 2 mM $(NH_4)_2MoS_4$ and 0.1 M phosphate buffer for electrodeposition of MoS_x by cycling the potential from 0.3 V to -1.3 V (*vs.* Ag/AgCl (3 M KCl)) at a scan rate of 50 mV s^{-1} for 10 times according to the procedure developed by Merki *et al.*[45]. During this process, GO is electroreduced to reduced graphene oxide (rGO), while MoS_x is electrodeposited onto the rGO. MoS_x, rGO-PEI, rGO-MoS_x, rGO-PEG-MoS_x and rGO-PDDA-MoS_x electrodes were prepared by a similar procedure. To prepare TEM samples, catalyst materials were carefully scraped off from the electrode surface and dispersed in water by sonication for 30 minutes. Afterwards, 2 μL of the dispersion was drop casted on a copper grid and dried in air.

Electrochemical measurements

Cyclic voltammetric (CV) measurements were carried out in 0.5 M aqueous $NaHCO_3$ solution saturated with N_2 or CO_2 by bubbling N_2 or CO_2 for at least 30 minutes in a conventional three-electrode cell comprising a platinum wire counter electrode, an Ag/AgCl (3 M KCl) reference electrode and a modified or unmodified GCE as the working electrode. In some experiments, a piece of high surface area carbon cloth (1 cm x 0.5 cm) modified with rGO-PEI-MoS_x was used as working electrode. For hydrogen evolution reaction (HER) catalysis, CV measurements were conducted in 0.5 M H_2SO_4, 0.5 M $NaHCO_3$ and 0.5 M phosphate buffer (pH 7.2) solutions, respectively, at a scan rate of 5 mV s^{-1} with iR compensation. Electrolysis at different applied potentials was performed in a gas-tight two-compartment electrochemical cell with a glass frit as the separator. Each compartment contained 12.5 mL electrolyte and approximately 20 mL headspace. A piece of carbon cloth (1cm x 1.5 cm) was used as counter electrode, an Ag/AgCl (3 M KCl) as reference electrode and a modified glassy carbon plate (0.4 cm x 1.5 cm) as working electrode. Before electrolysis, the cell was degassed by bubbling CO_2 gas for at least 30 min. The solutions in both compartment were stirred during electrolysis. After the electrolysis, a small fraction of the cell's head space products (200 μL) was sampled by gas-tight syringe and analysed by GC. For each electrolysis, the products were sampled and analysed twice in a very short time interval and two electrolysis experiments were run at each applied potential. The durability test was conducted by chronoamperometry at a constant potential of -0.65 V using a rGO-PEI-MoS_x modified 3 mm diameter GCE. A slightly positive CO_2 pressure was applied to prevent air from entering the electrolysis cell and to maintain the concentration of CO_2.

All potentials were converted to the reversible hydrogen electrode (RHE) reference scale using the formula: E (*vs*. RHE) = E (*vs*. Ag/AgCl) + 0.210 V + 0.059 V x pH. All the working electrodes were polished using a 0.3 μm aqueous alumina slurry on a polishing cloth, sonicated in water and acetone, rinsed with acetone, and then dried under a flow of nitrogen before use.

Results and discussion

Fourier Transform Infrared spectroscopic characterization of GO-PEI

Fourier Transform Infrared (FT-IR) spectroscopic characterization of GO and GO-PEI was undertaken to reveal the nature of the interaction between PEI and GO. As shown in Fig. 2a, these two materials exhibit distinctly different FT-IR spectra. Two additional peaks at 2841 and 2932 cm^{-1} were found with GO-PEI, which were assigned to symmetric and asymmetric stretching modes of the CH_2 of the PEI chains.[46] Furthermore, a significant decrease of the peak at 1724 cm^{-1} (attributed to C=O from the carboxyl group in pristine GO) and the appearance of a new band at 1632 cm^{-1} (attributed to the C=O stretching of the primary amide) suggest that the carbonyl

groups are converted to amides on reaction with the PEI.[47] This is further confirmed by the new bands observed at 1450 cm^{-1} (C-N stretching vibration) and 1572 cm^{-1} (N-H bending vibration) with GO-PEI.[48] This covalent interaction between PEI and GO is beneficial in maintaining the high stability of the modified electrode under long term electrolysis conditions. It is important to point out that the band at 1592 cm^{-1} ascribed to the C=C vibration of the aromatic rings was observed in both GO and GO-PEI, implying that the sp^2 character in GO-PEI is preserved after the chemical conjugation,[49] which is crucial to preserve the conductivity of the fabricated electrode.
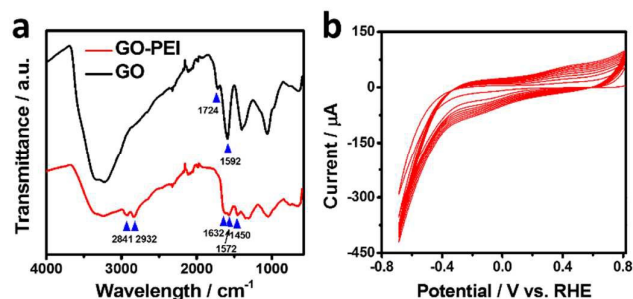
Fig. 2 (a) FT-IR spectra of GO (black line) and GO-PEI (red line). (b) Electrodeposition of rGO-PEI-MoS_x on GCE by repeating CVs for 10 cycles.

Fabrication and characterization of rGO-PEI-MoS_x

The rGO-PEI-MoS_x electrode was fabricated by electrodeposition of MoS_x onto a rGO-PEI modified electrode using the detailed procedure described in the Experimental section. The voltammogram (Fig. 2b) clearly demonstrates that a new reduction process at -0.1 V (*vs*. RHE, all potentials hereafter are with respect to this reference) and a new oxidation process at 0.4 V emerge and their current magnitude increases with cycling. The oxidation peak is attributed to the oxidation of $[MoS_4]^{2-}$ to form MoS_3 and S_8 according to the following equation:[50,51]

$$[MoS_4]^{2-} \rightarrow MoS_3 + \frac{1}{8}S_8 + 2e^-$$
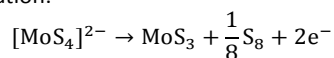
The reduction peak is assigned to the reduction of the electrogenerated S_8. In the potential region more negative than -0.25 V, reductive deposition of amorphous Mo^{IV}S$_2$ (i.e. MoS_x) takes place according to the previous electrochemical quartz crystal microbalance studies.[50]

$$[MoS_4]^{2-} + 2H_2O + 2e^- \rightarrow MoS_2 + 2HS^- + 2OH^-$$
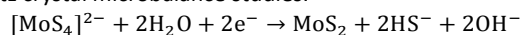
In the potential range of -0.4 V to -0.69 V, GO is electro-reduced to rGO.[52] Thus, the deposition of MoS_x and reduction of GO occurred simultaneously in this potential region, which was confirmed by energy dispersive spectroscopy (EDS) and Raman spectroscopy (Fig. S1). The presence of hydrophilic PEI on GO could increase the space between each GO layer and make it more easily accessible for $[MoS_4]^{2-}$ to achieve efficient deposition of MoS_x.[53] Moreover, both rGO-PEI and rGO-PEI-MoS_x modified GCE show a large increase in capacitance compared to bare GCE (Fig. S2) due to a significantly enlarged conductive surface area introduced by rGO.[54] The further enhanced capacitance of rGO-PEI-MoS_x arises from pseudo-

capacitance processes associated with MoS_x.[55] To confirm the interaction between rGO and MoS_x, transmission electron microscopic (TEM) and scanning electron microscopic (SEM) images were used to characterize the morphology. As revealed in Fig. S3, rGO-PEI-MoS_x shows a translucent and wrinkled texture associated with flexible graphene sheets. Fig. 3a shows the magnified image and MoS_x nanoparticles of diameter 17 ± 3 nm (Fig. S4) can be clearly seen. The fast Fourier transform (FFT) pattern indicates the amorphous nature of MoS_x nanoparticles (Fig. 3a insert), which is further confirmed by X-ray Diffraction (XRD, Fig. S5) with no characteristic peaks of any crystalline structures observed. Moreover, in the absence of GO-PEI, the MoS_x tended to aggregate into much larger particles (Fig. S6). By contrast, as can be seen from Fig. 3b, the MoS_x nanoparticles grew uniformly on the surface of rGO-PEI allowing the exposure of more active sites of MoS_x to CO_2.
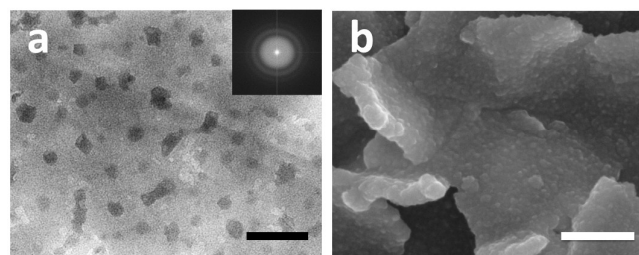
Fig. 3 TEM (a) and SEM (b) images of rGO-PEI-MoS_x. Insert of (a): corresponding FFT pattern. Scale bar: (a) 100 nm, (b) 200 nm.

CO_2 reduction activities of rGO-PEI-MoS_x

To assess the possibility of using rGO-PEI-MoS_x for electrocatalytic reduction of CO_2, CV studies were firstly undertaken in N_2-saturated and CO_2-saturated 0.5 M aqueous $NaHCO_3$ solutions (pH values 8.5 and 7.2, respectively) at a scan rate of 50 mV s^{-1} (Fig. 4a). Under both atmospheres, rapid increases of current were observed at around -0.22 V. In the more negative potential region, a broad process centred at -0.65 V appears under the CO_2 atmosphere. Similar processes were also reported in the previous studies with nitrogen-doped carbon nanofibers[16] or Ag[23,56] as the catalysts and were assigned to the reduction of CO_2. Since CV cannot provide conclusive evidence about the nature of this reduction process, potentiostatic electrolysis was conducted by applying a potential in the range of -0.25 V to -0.95 V (corresponding i-t curve is depicted in Fig. S7) and the faradaic efficiency (F.E.) is plotted as a function of the applied potential in Fig. 4b. The results reveal that H_2 and CO are the dominant products with a combined F.E. of around 100% over the whole potential range. Therefore, the liquid products, if any, were not analysed. The selectivity towards H_2 and CO is strongly dependent on the applied potential. At an applied potential of -0.25 V (corresponding to an overpotential of 140 mV for the formation of CO, since the equilibrium potential is -0.11 V vs. RHE[5]. All the overpotentials hereafter are reported with respect to this equilibrium potential.), CO with a F.E. of ~ 5% was detected while H_2 is the dominant product. This

overpotential for CO formation is significantly lower than that of polycrystalline Au or Ag[5] and as low as that achieved in oxide-derived Au nanoparticles under the same conditions.[20] F.E. of CO formation overtakes H_2 evolution when the potential becomes more negative and it reaches the maximum of 85.1% at an applied potential of -0.65 V (overpotential of 540 mV), which exceeds the highest F.E. of the polycrystalline Ag electrode reported in the same electrolyte medium.[5] H_2 regains dominance in the more negative potential region. This phenomenon was also observed in the case of Ag and Au catalysts in previous reports[5,27,56,57] and has been explained as follows: in the potential region of low CO_2/CO overpotentials, HER is dominant since it is thermodynamically and kinetically more favourable.[5,58] In the potential region of intermediate CO_2/CO overpotentials (i.e. -0.35 – -0.75 V vs. RHE), CO_2 reduction occurs to form CO, and HER is hindered due to the slow desorption of CO from the active sites.[59] In the potential region of high CO_2/CO overpotentials, kinetics of both CO_2 reduction and HER increase. However, HER regains dominance since H_2 evolution is the kinetically favoured process and H^+ is much more readily available in the aqueous HCO_3^- medium. Therefore, CO_2 reduction process becomes relatively slower due to either kinetic or mass transport limitations.[21,42,56,57]
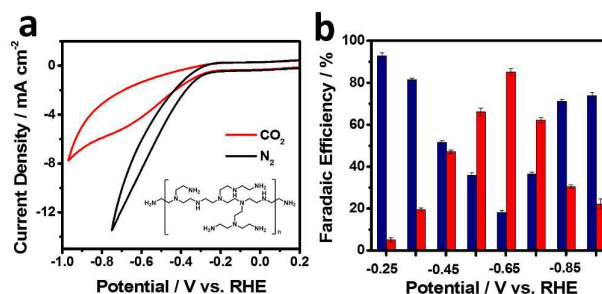
Fig. 4 (a) CVs of rGO-PEI-MoS_x modified GCE in N_2-saturated (black curve) and CO_2-saturated (red curve) 0.5 M aqueous $NaHCO_3$ solution. Scan rate was 50 mV s^{-1}. Insert: structure of PEI. (b) Faradaic efficiency for CO (red bars) and H_2 (blue bars) as a function of potential. Error bar associated with each value is also provided.

The source of CO is an important issue that needed to be confirmed. In our study, no CO was detected when the electrolysis was undertaken in a N_2 atmosphere, which confirms that the direct source of CO is not HCO_3^-. Another possible source could be the catalyst materials, which include support electrode, rGO and PEI. ^{13}C labelled CO_2 and $NaHCO_3$ could be used to provide direct evidence. However, the formal potential is 0.52 V vs. RHE for the reaction CO (g) + $2H^+$ + $2e^-$ ↔ C(s) + H_2O, which is much more positive than the applied potential (-0.25 – -0.95 V vs. RHE) used in our studies. Therefore, direct oxidation of C to generate CO is not a thermodynamically favorable process. Under the mildly reducing electrochemical conditions involved in our work, extensive oxidation of rGO and PEI to produce the amount of CO detected is also very unlikely. Moreover, we also measured the weight difference of the rGO-PEI-MoS_x modified glassy

         ARTICLE

carbon plate electrode before and after electrolysis (see Note S1 in the ESI for detail) and found that the weight loss is far less than the amount needed to supply the CO produced during electrolysis. Even carbon with the same mass as all of the modified catalyst materials cannot produce sufficient CO at 100% conversion yield. Therefore, neither rGO nor PEI can be the major source of CO.

The intrinsic catalytic activity toward CO_2 reduction for each MoS_x active site is indicated by turnover frequency (TOF), calculated using the following equation:

$$TOF = \frac{I_{total}F.E.}{2Fn}$$

where I_{total} is the current (in A) in CV measurement, F.E. is faradaic efficiency for CO formation, n is active sites number (in mol) and F is Faraday's constant (in C mol^{-1}). The factor 2 arises from the fact that two electrons are required to form one CO molecule from one CO_2 molecule. Taking I_{total} = 3.4 x 10^{-4} A, F.E. = 85.1%, n = 6.18 x 10^{-10} mol (estimated from voltammetric measurements, Fig. S8), the TOF at the applied potential of -0.65 V is calculated to be 2.4 s^{-1}. Such a large TOF value implies that this catalyst could potentially be used for practical applications when it is immobilized on a porous support with a large surface area. Indeed, a current density as high as 55 mA cm^{-2} at -0.65V could be reached when the rGO-PEI-MoS_x composite catalyst was immobilized on a carbon cloth electrode (Fig. S9).

It is also worth noting that the molar ratio of H_2 and CO is about 2:1, which is the composition of syngas, when the applied potential is -0.4 V (equivalent to 290 mV overpotential for CO formation) (Fig. 5). Thus, this produced gas mixture could readily serve as the source gas for the Fischer-Tropsch process, an important gas to liquids technology for generating methanol, synthetic petroleum and other liquid fuels.[28] More importantly, the F.E. of H_2 and CO remains constant at this potential over at least 3 hours of electrolysis (Fig. 5), showing great promise as a practical catalyst for this process.
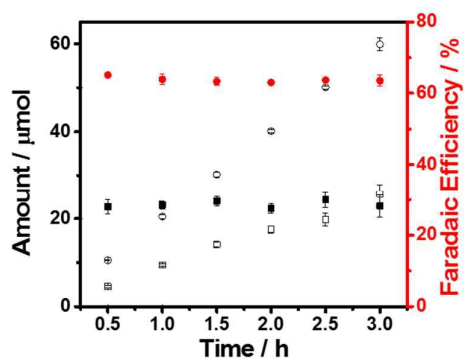
Fig. 5 Amount and faradaic efficiency of H_2 (circles) and CO (squares) with error bars. Potentiostatic electrolysis at -0.4 V in CO_2-saturated 0.5 M aqueous $NaHCO_3$ solution. Measurement interval: 0.5 h.

In addition, the durability of rGO-PEI-MoS_x was also studied by chronoamperometry at -0.65 V, which is the optimum potential with respect to maximum CO selectivity. As shown in Fig. S10, the current remains stable in the time scale of 16 hours (60,000 s). Initial decay of current, which cannot be completely attributed to the double layer charging process, is mainly due to the adsorption of gaseous products. This current was largely recovered when the electrode was left under open circuit condition for 500 seconds before applying the same potential for electrolysis, suggesting long-term durability of the rGO-PEI-MoS_x. SEM images and EDS of the electrode surface after 60,000 s are shown in Fig. S11. Compared with SEM image taken before the electrolysis (Fig. 3b), not much difference in morphology was observed after the long-term electrolysis experiment. The elemental analysis reveals the preservation of C, N, Mo and S elements, which also indicates the stability of the material. In HER catalysis, amorphous MoS_x often suffers from activity decay due to mechanical loss of catalyst materials or poisoning by surface adsorbates from the electrolyte or reference electrode rather than inherent property changes.[60,61] Chorkendorff *et al.* showed that catalyst support, such as carbon fibers, could play an important role in improving the mechanical stability of the amorphous MoS_x catalyst.[62] Therefore, in our case, the presence of the rGO support enhances the mechanical stability of the electrodes under catalytic turnover conditions, as suggested in regard to other types of support.[55,62-64]

Possible origins of the activity of rGO-PEI-MoS_x for CO_2 reduction

To reveal the possible origins of the activity of rGO-PEI-MoS_x for CO_2 reduction, the CV measurements were undertaken using rGO-PEI, rGO-MoS_x and rGO-PEI-MoS_x modified GCEs, respectively. As shown in Fig. 6a, in the absence of MoS_x, rGO-PEI modified GCE demonstrates a reduction onset potential that is about 500 mV more negative than the other two electrodes in both N_2-saturated and CO_2-saturated 0.5 M aqueous $NaHCO_3$ solutions which indicates that MoS_x is the effective catalyst towards the reduction reactions observed here. Electrolysis results (Fig. 6b) show only H_2 was detected with a F.E. of ~93% at -0.85 V. The rGO-MoS_x modified GCE presents similar CV curves in N_2 and CO_2 atmospheres and potentiostatic electrolysis at -0.65 V reveals that H_2 is the only product with a F.E. of ~95%. Interestingly, although the incorporation of PEI into rGO-MoS_x system results in a decrease in current density under either N_2 or CO_2 atmospheres, which will be discussed later, there is a significant difference in voltammetric characteristics and a considerably higher F.E. for CO at -0.65 V. Hence, a synergetic effect of PEI and MoS_x is responsible for the catalysis of CO_2 reduction.
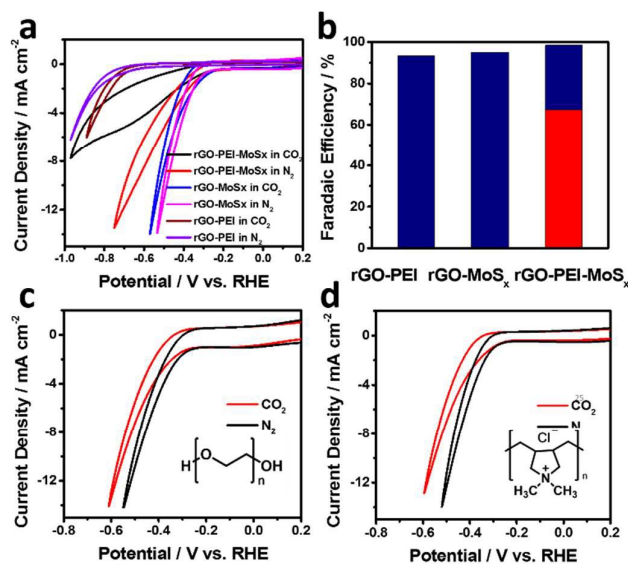
Fig. 6 (a) CVs of rGO-PEI, rGO-MoS$_x$, rGO-PEI-MoS$_x$ modified GCE in N$_2$-saturated and CO$_2$-saturated 0.5 M aqueous NaHCO$_3$ solution. Scan rate was 50 mV s^{-1}. (b) Faradaic efficiency for CO (red bar) and H$_2$ (blue bars) of rGO-PEI, rGO-MoS$_x$, rGO-PEI-MoS$_x$, potentiostatic electrolysis at -0.65 V in CO$_2$-saturated 0.5 M aqueous NaHCO$_3$ solution. CVs of rGO-PDDA-MoS$_x$ (c) and rGO-PEG-MoS$_x$ (d) modified GCE in N$_2$-saturated and CO$_2$-saturated 0.5 M aqueous NaHCO$_3$ solution. Scan rate was 50 mV s^{-1}. Insert of (c) and (d) shows the structure of PDDA and PEG, respectively.

Crystalline MoS$_2$ has demonstrated its capability for effectively electroreducing CO$_2$ in an imidazolium based IL mixed with water as proton source.[42] Similar observations have also been made previously by the same group in their study of electrocatalytic reduction of CO$_2$ at an Ag electrode in this medium.[65] They found that imidazolium cation could act as a cocatalyst via the formation of IL-CO$_2$ complex to reduce the activation energy barrier. Nørskov *et al.* recently predicted theoretically by DFT calculations that the edge sites of crystalline MoS$_2$ could be the catalysing sites for CO$_2$ reduction.[41] They claimed that the bridging S atom at the edges of MoS$_2$ could selectively bind the intermediate HCOO over the product CO, which resulted in a deviation from the transition-metal scaling relationship of intermediates in CO$_2$ reduction process and therefore significantly improved CO$_2$ reduction activities over transition-metal catalysts. Although there are no well-defined edges in amorphous MoS$_x$, there are many structurally and coordinatively unsaturated Mo and S atoms,[45,61,66] which are equivalent to the edge sites in crystalline from a catalysis point of view. On this basis, in principle, the amorphous MoS$_x$ used in our study may be expected to be a better electrocatalyst for CO$_2$ reduction due to its abundance of such active sites.

However, in the absence of PEI, rGO-MoS$_x$ modified GCE only showed activity towards HER, which infers the crucial role of PEI for CO$_2$ reduction. To investigate its role, PEI was replaced with other polymers, poly diallyldimethylammonium

chloride (PDDA) or polyethylene glycol (PEG) for the fabrication of rGO-polymer-MoS$_x$ modified electrodes. Fig. 6c and d present the CVs of rGO-PDDA-MoS$_x$ and rGO-PEG-MoS$_x$ modified GCE in N$_2$-saturated and CO$_2$-saturated 0.5 M aqueous NaHCO$_3$ solution at the scan rate of 50 mV s^{-1}, respectively. Again, both electrodes show similar CV curves in N$_2$ and CO$_2$ atmospheres with the same onset potential and only a slight decrease of current density in the present of CO$_2$ and further potentiostatic electrolysis demonstrated H$_2$ as the only product. Thus it is clear that the PEI possesses unique properties that produce synergetic effects with MoS$_x$ for CO$_2$ reduction. Two factors may account for this effect:

(1) PEI can suppress HER and thus enhance the competing CO$_2$ reduction. To probe this further, the HER catalysis properties of rGO-MoS$_x$ and rGO-PEI-MoS$_x$ were investigated in aqueous media, containing 0.5 M H$_2$SO$_4$, 0.5 M bicarbonate (pH 8.5) or 0.5 M phosphate buffer (pH 7.2, at which catalytic CO$_2$ reduction was observed in our study). Results obtained are shown in Fig. S12. The kinetics of HER reaction were retarded in the presence of PEI in all media, as suggested by a larger overpotential. This effect of PEI on the HER is most likely due its amine groups. Rezaei *et al.* have shown that amine groups in ionic liquids electrolytes can inhibit hydrogen formation in aqueous H$_2$SO$_4$ solution.[67] Rosen *et al.* also found this effect when they used an ionic liquid as a co-catalyst for CO$_2$ reduction in mixed solvents containing water and [EMIM][BF$_4$].[68]

(2) PEI may stabilize the intermediate species in the CO$_2$ reduction process. Tafel slopes of ~ 120 mV dec^{-1} have often been reported in the previous studies in aqueous media at metallic electrodes since the one-electron reduction of CO$_2$ to form CO$_2$$^{.-}$ is the rate determining step.[5] By contrast, a much smaller value of 74 mV dec^{-1} was obtained with our rGO-PEI-MoS$_x$ modified electrode in the present work (Fig. S13). Considering the presence of a competing HER, this value is close to the theoretical value of 59 mV dec^{-1} predicted for the case where a reversible CO$_2$/CO$_2$$^{.-}$ process occurs prior to a rate-determining chemical step.[7,20,21] This enhanced kinetics of the CO$_2$/CO$_2$$^{.-}$ process was attributed in studies of N-doped carbon nanotubes, to the stabilization of CO$_2$$^{.-}$ by the amines on PEI, through hydrogen bonding and electrostatic interactions.[43]

Conclusions

In summary, we have synthesized amorphous molybdenum sulphide (MoS$_x$) on polyethylenimine (PEI) modified reduced graphene oxide (rGO-PEI-MoS$_x$) and used it as a heterogeneous catalyst for electrocatalytic reduction of CO$_2$ to CO in CO$_2$ saturated aqueous NaHCO$_3$ solution with high efficiency and selectivity. The catalyst is capable of reducing CO$_2$ to CO at an overpotential as low as 140 mV. It reaches a maximum faradaic efficiency of 85.1% at an overpotential of 540 mV, under which this catalyst exhibits a high TOF value of 2.4 s^{-1} for the formation of CO. Consequently, when the catalyst was deposited on the porous carbon cloth electrode with a large active surface area, a current density of about 50

mA cm^{-2} can be reached at the same overpotential. At an overpotential of only 290 mV with respect to CO formation, this catalyst is also capable of producing syngas. The catalyst is highly stable in the long-term electrolysis. The efficiency and selectivity towards CO_2 reduction rather than hydrogen evolution at the optimal applied potential are attributed to the synergetic combination of the properties of MoS_x and PEI. Our promising rGO-PEI-MoS_x composite catalyst may pave a new way for efficient CO_2 reduction catalysis based on inexpensive noble-metal-free materials. Catalytic performance could be further improved by finely tune the properties of MoS_2 using the well-established doping methods.[39,51,69]

Acknowledgements

Notes and references

1. N. S. Lewis and D. G. Nocera, *Proc. Natl. Acad. Sci. USA*, 2006, **103**, 15729-15735.
2. H. A. Gasteiger and N. M. Markovic, *Science*, 2009, **324**, 48-49.
3. T. A. Faunce, W. Lubitz, A. W. Rutherford, D. R. MacFarlane, G. F. Moore, P. Yang, D. G. Nocera, T. A. Moore, D. H. Gregory, S. Fukuzumi, K. B. Yoon, F. A. Armstrong, M. R. Wasielewski and S. Styring, *Energy Environ. Sci.*, 2013, **6**, 695-698.
4. J. Qiao, Y. Liu, F. Hong and J. Zhang, *Chem. Soc. Rev.*, 2014, **43**, 631-675.
5. Y. Hori, in *Modern aspects of electrochemistry*, Springer, 2008, 89-189.
6. J. Schneider, H. Jia, J. T. Muckerman and E. Fujita, *Chem. Soc. Rev.*, 2012, **41**, 2036-2051.
7. Y. Chen and M. W. Kanan, *J. Am. Chem. Soc.*, 2012, **134**, 1986-1989.
8. Y. Oh, H. Vrubel, S. Guidoux and X. Hu, *Chem. Commun.*, 2014, **50**, 3878-3881.
9. C. W. Li and M. W. Kanan, *J. Am. Chem. Soc.*, 2012, **134**, 7231-7234.
10. M. R. Dubois and D. L. Dubois, *Acc. Chem. Res.*, 2009, **42**, 1974-1982.
11. C. Costentin, M. Robert and J. -M. Savéant, *Chem. Soc. Rev.*, 2013, **42**, 2423-2436.
12. I. Bhugun, D. Lexa and J. -M. Savéant, *J. Am. Chem. Soc.*, 1996, **118**, 1769-1776.
13. S. Lin, C. S. Diercks, Y. B. Zhang, N. Kornienko, E. M. Nichols, Y. Zhao, A. R. Paris, D. Kim, P. Yang and O. M. Yaghi, *Science*, 2015, **349**, 1208-1213.
14. Y. Oh and X. Hu, *Chem. Soc. Rev.*, 2013, **42**, 2253-2261.
15. E. Barton Cole, P. S. Lakkaraju, D. M. Rampulla, A. J. Morris, E. Abelev and A. B. Bocarsly, *J. Am. Chem. Soc.*, 2010, **132**, 11539-11551.
16. B. Kumar, M. Asadi, D. Pisasale, S. Sinha-Ray, B. A. Rosen, R. Haasch, J. Abiade, A. L. Yarin and A. Salehi-Khojin, *Nature Commun.*, 2013, **4**, 2819-2826.
17. Y. Liu, S. Chen, X. Quan and H. Yu, *J. Am. Chem. Soc.*, 2015, **137**, 11631-11636.
18. K. P. Kuhl, T. Hatsukade, E. R. Cave, D. N. Abram, J. Kibsgaard and T. F. Jaramillo, *J. Am. Chem. Soc.*, 2014, **136**, 14107-14113.
19. X. Min and M. W. Kanan, *J. Am. Chem. Soc.*, 2015, **137**, 4701-4708.
20. Y. Chen, C. W. Li and M. W. Kanan, *J. Am.Chem. Soc.*, 2012, **134**, 19969-19972.
21. Q. Lu, J. Rosen, Y. Zhou, G. S. Hutchings, Y. C. Kimmel, J. G. Chen and F. Jiao, *Nature Commun.*, 2014, **5**, 3242-3247.
22. Q. Lu, J. Rosen and F. Jiao, *ChemCatChem*, 2014, **7**, 38-47.
23. S.-K. Amin, J. Huei-Ru, A. R. Brian, Z. Wei, M. Sichao, J. A. K. Paul and I. M. Richard, *J. Phys. Chem. C*, 2013, **117**, 1627-1632.
24. D. Gao, H. Zhou, J. Wang, S. Miao, F. Yang, G. Wang, J. Wang and X. Bao, *J. Am. Chem. Soc.*, 2015, **137**, 4288-4291.
25. W. Zhu, R. Michalsky, O. Metin, H. Lv, S. Guo, C. J. Wright, X. Sun, A. A. Peterson and S. Sun, *J. Am. Chem. Soc.*, 2013, **135**, 16833-16836.
26. W. Zhu, Y. J. Zhang, H. Zhang, H. Lv, Q. Li, R. Michalsky, A. A. Peterson and S. Sun, *J. Am. Chem. Soc.*, 2014, **136**, 16132-16135.
27. C. Kim, H. S. Jeon, T. Eom, M. S. Jee, H. Kim, C. M. Friend, B. K. Min and Y. J. Hwang, *J. Am. Chem. Soc.*, 2015, DOI: 10.1021/jacs.5b06568.
28. Y. Zhang, G. Jacobs, D. E. Sparks, M. E. Dry and B. H. Davis, *Catal. Today*, 2002, **71**, 411-418.
29. C. W. Li and M. W. Kanan, *J. Am. Chem. Soc.*, 2012, **134**, 7231-7234.
30. S. Zhang, P. Kang and T. J. Meyer, *J. Am. Chem. Soc.*, 2014, **136**, 1734-1737.
31. J. L. DiMeglio and J. Rosenthal, *J. Am. Chem. Soc.*, 2013, **135**, 8798-8801.
32. J. Medina-Ramos, J. L. DiMeglio and J. Rosenthal, *J. Am. Chem. Soc.*, 2014, **136**, 8361-8367.
33. J. C. Boyington, V. N. Gladyshev, S. V. Khangulov, T. C. Stadtman and P. D. Sun, *Science*, 1997, **275**, 1305-1308.
34. K. Schuchmann and V. Müller, *Science*, 2013, **342**, 1382-1385.
35. T. Reda, C. M. Plugge, N. J. Abram and J. Hirst, *Proc. Natl. Acad. Sci. USA*, 2008, **105**, 10654-10658.
36. A. Bassegoda, C. Madden, D. W. Wakerley, E. Reisner and J. Hirst, *J. Am. Chem. Soc.*, 2014, **136**, 15473-15476.
37. B. Hinnemann, P. G. Moses, J. Bonde, K. P. Jørgensen, J. H. Nielsen, S. Horch, I. Chorkendorff and J. K. Nørskov, *J. Am. Chem. Soc.*, 2005, **127**, 5308-5309.
38. T. F. Jaramillo, K. P. Jørgensen, J. Bonde, J. H. Nielsen, S. Horch and I. Chorkendorff, *Science*, 2007, **317**, 100-102.
39. M. Chhowalla, H. S. Shin, G. Eda, L.-J. Li, K. P. Loh and H. Zhang, *Nature Chem.*, 2013, **5**, 263-275.
40. J. D. Benck, T. R. Hellstern, J. Kibsgaard, P. Chakthranont and T. F. Jaramillo, *ACS Catal.*, 2014, **4**, 3957-3971.
41. K. Chan, C. Tsai, H. A. Hansen and J. K. Nørskov, *ChemCatChem*, 2014, **6**, 1899-1905.
42. M. Asadi, B. Kumar, A. Behranginia, B. A. Rosen, A. Baskin, N. Repnin, D. Pisasale, P. Phillips, W. Zhu, R. Haasch, R. F. Klie, P. Kral, J. Abiade and A. Salehi-Khojin, *Nature Commun.*, 2014, **5**, 4470-4477.
43. S. Zhang, P. Kang, S. Ubnoske, M. K. Brennaman, N. Song, R. L. House, J. T. Glass and T. J. Meyer, *J. Am. Chem. Soc.*, 2014, **136**, 7845-7848.
44. W. S. Hummers and R. E. Offeman, *J. Am. Chem. Soc.*, 1958, **80**, 1339-1339.

45. D. Merki, S. Fierro, H. Vrubel and X. Hu, *Chem. Sci.*, 2011, **2**, 1262-1267.

46. Y. Zhang, B. Chen, L. Zhang, J. Huang, F. Chen, Z. Yang, J. Yao and Z. Zhang, *Nanoscale*, 2011, **3**, 1446-1450.

47. X. Zhou, Z. Chen, D. Yan and H. Lu, *J. Mater. Chem.*, 2012, **22**, 13506-13516.

48. Z. Y. Sui, Y. Cui, J. H. Zhu and B. H. Han, *ACS Appl. Mater. Inter.*, 2013, **5**, 9172-9179.

49. H. Kim, R. Namgung, K. Singha, I. K. Oh and W. J. Kim, *Bioconj. Chem.*, 2011, **22**, 2558-2567.

50. H. Vrubel and X. Hu, *ACS Catal.*, 2013, **3**, 2002-2011.

51. C. G. Morales-Guio and X. Hu, *Acc. Chem. Res.*, 2014, **47**, 2671-2681.

52. S. -X. Guo, S. -F. Zhao, A. M. Bond and J. Zhang, *Langmuir*, 2012, **28**, 5275-5285.

53. X. Yang, C. Cheng, Y. Wang, L. Qiu and D. Li, *Science*, 2013, **341**, 534-537.

54. F. Li, J. Chen, X. Wang, M. Xue and G. Chen, *Adv. Funct. Mater.*, 2015, **25**, 4601-4606.

55. Z. Pu, Q. Liu, A. M. Asiri, A. Y. Obaid and X. Sun, *J. Power Sources.*, 2014, **263**, 181-185.

56. T. Hatsukade, K. P. Kuhl, E. R. Cave, D. N. Abram and T. F. Jaramillo, *Phys. Chem. Chem. Phys.*, 2014, **16**, 13814-13819.

57. Y. Hori, A. Murata, K. Kikuchi and S. Suzuki, *J. Chem. Soc., Chem. Commun.*, 1987, **10**, 728-729.

58. C. Delacourt, Charles, P. L. Ridgway and J. Newman, *J. Electrochem. Soc.*, 2010, **157**, B1902-B1910.

59. P. Kedzierzawski and J. Augustynski, *J. Electrochem. Soc.*, 1994, **141**, L58-L60.

60. D. Merki, H. Vrubel, L. Rovelli, S. Fierro and X. Hu, *Chem. Sci.*, 2012, **3**, 2515-2525.

61. J. D. Benck, Z. Chen, L. Y. Kuritzky, A. J. Forman and T. F. Jaramillo, *ACS Catal.*, 2012, **2**, 1916-1923.

62. A. B. Laursen, P. C. Vesborg and I. Chorkendorff, *Chem. Commun.*, 2013, **49**, 4965-4967.

63. D. J. Li, U. N. Maiti, J. Lim, D. S. Choi, W. J. Lee, Y. Oh, G. Y. Lee and S. O. Kim, *Nano Lett.*, 2014, **14**, 1228-1233.

64. S. Chen, J. Duan, Y. Tang, B. Jin and S. Z. Qiao, *Nano Energy*, 2015, **11**, 11-18.

65. B. A. Rosen, A. Salehi-Khojin, M. R. Thorson, W. Zhu, D. T. Whipple, P. J. Kenis and R. I. Masel, *Science*, 2011, **334**, 643-644.

66. H. Vrubel, D. Merki and X. Hu, *Energy Environ. Sci.*, 2012, **5**, 6136-6144.

67. B. Rezaei, S. Mallakpour and M. Taki, *J. Power Sources*, 2009, **187**, 605-612.

68. B. A. Rosen, W. Zhu, G. Kaul, A. Salehi-Khojin and R. I. Masel, *J. Electrochem. Soc.*, 2012, **160**, H138-H141.

69. Y. Sun, S. Gao, F. Lei and Y. Xie, *Chem. Soc. Rev.*, 2015, **44**, 623-636.

Energy & Environmental Science Accepted Manuscript

TOC figure

Energy & Environmental Science Accepted Manuscript